DOI: 10.1002/ejic.200900151

# Ion-Pairing in Organometallic Chemistry: Structure and Influence on Proton Transfer from a Computational Perspective

**Eric Clot*[a]**

*Dedicated to Odile Eisenstein on the occasion of her 60th birthday*

**Keywords:** Ion pairs / Density functional calculations / Anions / Cations / Proton transfer

The development of NMR spectroscopic techniques such as the nuclear Overhauser effect (NOE) and pulsed gradient spin echo (PGSE) method to study ion-pairing phenomena has increased the understanding of anion–cation interactions in organometallic chemistry and its influence on reactivity in homogeneous catalysis. These developments have greatly benefited from computational studies carried out in synergy with experimental observations. A good description of the preferred sites for anion interaction is obtained with charge analysis on the cation itself. However, depending on the nature of the anion, different geometries are likely to be observed, and only explicit calculations of the ion-pair structures allow discrimination between the different possibilities. Such ion pairs may alter the relative energy of isomers and/or stabilize transition states associated to a given pathway, thus leading to anion control of the reactivity in some instances.



## Introduction

In the past years, to gain a better understanding of the structure and reactivity of transition-metal complexes, much attention has been paid to the investigation of metal–ligand interactions. Emphasis is generally put on a given functional group involved in a targeted transformation (alkylidene for olefin metathesis, for example), and the reactivity of the complex is tuned by appropriate modification of the ancillary ligands and/or substitution of the functional group. Quite often, the catalytically active complex turns out to be cationic, and the counterion, which is not directly bound in the first coordination sphere, is generally considered to be an innocent partner. In recent years, however, the counterion has been recognized also to play a key role in the performance of the catalytic machinery on a molecular level. In this respect, the stabilization of ion pairs, the relative locations and orientations of the ions, as well as the overall dimensions of the ion-pair assembly are very important aspects that contribute to the understanding of the structure–activity relationships.[1,2]

The ion-pairing phenomenon has been deeply studied in the single-site early-transition-metal-catalyzed polymerization of alkenes.[3] It is now well established that the counterion significantly influences the catalytic activity, stability, kinetic profile of the polymerization, as well as the molecular weight and stereoregularity of the polymer. The influence of the counterion on the various steps of the polymerization process has been addressed computationally in a large number of papers.[4–8] However, in the particular case of alkene polymerization, the counterion is by definition

[a] Université Montpellier 2, Institut Charles Gerhardt, CNRS 5253,
Place Eugène Bataillon, 34095 Montpellier, France
Fax: +33-4-67144839
E-mail: eric.clot@univ-montp2.fr

*Eric Clot was born in Marseilles, France, in 1967. He graduated in physical chemistry from the Ecole Normale Supérieure de Lyon in 1992. He received his Ph.D. degree in Theoretical Chemistry in 1995 from the Université Paris-Sud Orsay under the supervision of Odile Eisenstein. After a postdoctoral stay of one year with Philippe Sautet in Lyon, he became a CNRS Chargé de Recherches (Research Associate) at the Université Montpellier 2 in 1996. In 2007, he was promoted to Directeur de Recherches (Research Director). His main research interest is the computational study of the structure and reactivity of organometallic complexes with particular emphasis on the description of the complexity of the catalytic system.*

  

non-innocent, as it is formed after activation of the catalyst by the co-catalyst. The geometry of the ion pair is therefore more or less dictated by the nature of the activation process. A typical example is the result of the reaction of $[Cp^*_2Zr(Me)_2]$ ($Cp^* = \eta^5$-$C_5Me_5$) with $B(C_6F_5)_3$, yielding the inner sphere ion pair (ISIP) $[(Cp^*_2ZrMe^+)\{MeB(C_6F_5)_3^-\}]$ (Scheme 1), whose X-ray structure has been determined.[9]

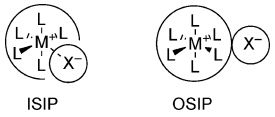


Scheme 1. Schematic representation of the inner sphere ion pair (ISIP) and the outer sphere ion pair (OSIP).

In processes other than olefin polymerization, the situation is dramatically different for typical cationic complexes whose counterion is generally considered as a negative charge present somewhere around the complex to ensure electroneutrality. In such an outer sphere ion pair (OSIP, Scheme 1), there is no direct interaction between the anion and the metal. Moreover, in the design of active cationic catalysts, interaction of the anion with the metal is a process that is likely to block potential active sites. The lack of reactivity and non-nucleophilic character of $BF_4^-$ and $PF_6^-$ have thus led to their widespread use as noncoordinating (or weakly coordinating) counterions supporting cationic organometallic complexes. With the generation of sufficiently electrophilic complexes, the limitations of $BF_4^-$ and $PF_6^-$ as nonreactive entities are encountered. To circumvent this problem, tetraarylborate anions, $BAr_4^-$ {Ar = Ph, $C_6F_5$, 3,5-$(CF_3)_2C_6H_3$}, are generally used. However, the question remains whether, in such OSIPs, the anion floats indifferently around the cation, or a specific ion-pair geometry is favoured as a result of the nature of the anion and the ligand set.

In the last ten years, nuclear Overhauser effect (NOE) NMR spectroscopic experiments coupled with pulsed gradient spin echo (PGSE) diffusion methods have given access to a wealth of information on the geometry and stability of ion pairs.[1,2] However, detailed information on the structure and on the strength of ion pairs is not available from NMR spectroscopic measurements. For example, it is difficult to relate accurately the intensity of the NOE peaks to any particular geometrical parameters. Computational studies are in this respect a very valuable tool, as different geometries for the ion pairs can be tested and compared to the experimental results. Also available from the calculations are the estimation of the stability of the ion pair with respect to separated ions and the characterization of the interactions at the origin of the formation of a given ion-pair structure (H-bonding, dispersive forces, for example). In particular, when inorganic fluorinated anions are considered, the counterion can be engaged in H-bonding interactions with the acidic sites on the ligands. This type of interaction can trigger the system toward a given geometry, but it may also influence the reactivity of the complex in processes associated with proton transfer.

The aim of this contribution is to review the calculations we have been performing in collaboration with the group of Alceo Macchioni to study the structure and energetics of ion pairs of cationic transition-metal complexes and dimers of some neutral complexes.[10] This has led us to study in some instances the influence of the counterion on proton transfer processes in the coordination sphere of iridium complexes.[11]

## 1. Structure of the Ion Pair

### 1.1. Charge Analysis of the Cation Alone

The structures of ion pairs have sometimes been inferred from X-ray structural work, where it is assumed that the solution structure, the only structure relevant to reactivity in solution, is the same as that in the solid state. However, the structure observed in the solid state is also dictated by close packing considerations where the anion is expected to occupy the least sterically encumbered position. Such a position would allow the shortest metal–anion separation, expected to be the preferred situation in formalism where the positive charge of the cation is carried by the metal centre.

A comparative study of the X-ray and solution structures of $[Ir(bipy)(H)_2(PPh_3)_2]X^-$ (X = $PF_6$, $BF_4$, $CF_3SO_3$, $BPh_4$; see Scheme 2) indicated that the anion can bind in an unexpected region of the cation.[10a] The assignments of all the $^1H$ and $^{13}C$ resonances were performed by following the scalar and dipolar nuclear interactions in the $^1H$ COSY, $^1H$,$^{13}C$ HMQC and $^1H$ NOESY experiments (Scheme 2). The relative anion–cation position of complexes **1** was investigated in $CD_2Cl_2$. Under these conditions, the complexes are mainly present in solution as intimate ion pairs, and dipolar interaction between nuclei belonging to the two ionic moieties can be detected in the $^1H$ NOESY or $^{19}F$,$^1H$ HOESY spectra. The nuclei of the counterions of complexes **1** interact essentially with the protons of the bipy ligand, and the strongest interactions are observed with the protons H3 and H3′, indicative of selective formation of the geometry shown in Scheme 2 for the ion pair. No contact is observed with the two hydrides H1′′ and H2′′. This is truly independent of the nature of the counterion and is in marked contrast with the results from the X-ray crystallographic characterization of compounds **1b** and **1c**.[12] The outer sphere anions $X^-$ are located close to the H6, H5 and H1′′, but far from the H6′, H5′ and H2′′ positions.

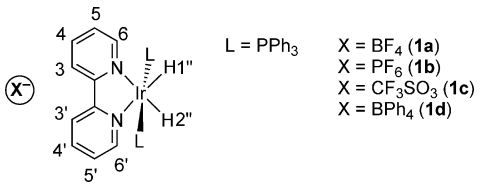


Scheme 2. Selective ion-pairing in $[Ir(bipy)(H)_2(L)_2]X$.

  

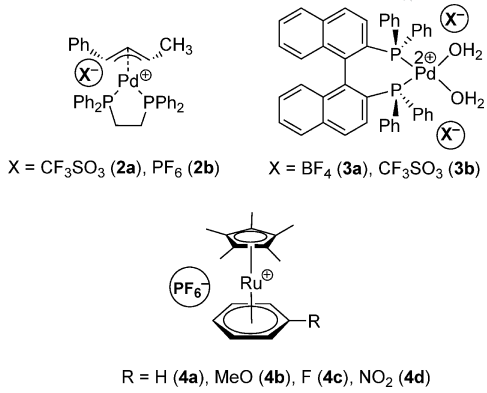


Scheme 3. Other examples of selective ion-pairing.

To elucidate the difference between the solution and solid-state structures, the geometry of $Ir(bipy)(H)_2(PPh_3)_2^+$ was optimized at the ONIOM(B3PW91/UFF) level. This hybrid quantum mechanics/molecular mechanics (QM/MM) approach has been shown to give good results in complexes where some dispersive interactions are expected between the ligands.[13] A natural population analysis (NPA) indicated that the positive charge is not localized on the $IrH_2$ part of the molecule. The NPA charges on the hydrides are –0.015 and –0.026, indicating a weak hydride character, while the metal is negatively charged (–0.13). In fact, because of the electronegative nature of the bipy nitrogen atoms (–0.55), the positive charge is accumulated on the carbon atoms C2 and C2′ (+0.21), forming the bond between the two rings. As a result, the dipole moment of the molecule lies in the bipy plane and bisects the C2–C2′ bond, the positive end of the dipole pointing away from the metal. This electronic distribution explains the results of the NMR spectroscopic studies where the anion is situated in the region maximizing the electrostatic interaction with the cation. Calculation of the electrostatic potential clearly indicated that the region between H3 and H3′ is associated with high positive values of the potential (or extension further away of a given contour value).

The formation of ion-pairing with selective geometry of cation–anion interactions has also been studied by Pregosin et al. on various $Pd^{II}$ and $Ru^{II}$ salts (Scheme 3).[14] The $^{19}F,^1H$ HOESY studies of the salts $[Pd(\eta^3\text{-}CH_3CHCHCHPh)(dppe)][X]$ {dppe = 1,2-bis(diphenylphosphanyl)ethane, $X = CF_3SO_3^-$, $PF_6^-$} in chloroform revealed a selective approach of the anion with respect to the allyl ligand (**2a** and **2b**, Scheme 3).[14a] The anion approaches the Pd centre from the side of the two terminal protons and is somewhat closer to the allyl phenyl ring than to the allyl methyl group. DFT(B3LYP) calculations were carried out on the model $Pd(\eta^3\text{-}CH_3CHCHCHPh)(Me_2PCH_2CH_2PMe_2)^+$. The NPA charges on the terminal allyl carbons do not differ much (–0.29), whereas the Pd atom is positively charged (+0.286). The difference between the two substituents of the allyl ligand is illustrated by the much less negative charge on the phenyl *ipso* carbon of the phenyl ring (–0.086) compared to the charge on the methyl carbon (–0.696). Thus the selective approach observed for the anion is explained by electrostatic considerations with the positive charge on the metal and the less negative part of the allyl toward the phenyl group.

In another study, the dicationic complex $[Pd(H_2O)_2(BINAP)]^{2+}$ was studied with $BF_4^-$ and $CF_3SO_3^-$ as counterion (**3a** and **3b** in Scheme 3).[14b] The $^{19}F$, $^1H$ HOESY spectrum of **3a** reveals a strong contact to the water molecules and a medium strength contact to the equatorial P–phenyl aromatic protons of the BINAP ligand. For salts **3b**, the strongest contact is with the equatorial P–phenyl aromatic protons, whereas the contact from the $CF_3SO_3$ fluorine to the water is rather weak. The difference was rationalized by invoking different H-bonding interactions, F···$H_2O$ in the case of **3a** and O···$H_2O$ in the case of **3b**. The geometry of the cation was optimized at the B3LYP level, and the NPA charge distribution revealed that the phosphorus atoms bear significantly larger positive charge (+1.30) than the Pd atom (+0.37). Although these results should not be taken as quantitative, they indicate that the anion is expected to seek out the P atoms preferentially. However, the calculations performed do not account for the H-bonding between the anion and the coordinated water molecules.

The $^{19}F,^1H$ HOESY study of the $PF_6^-$ salts of the cation $[Ru(Cp^*)(\eta^6\text{-}C_6H_5R)]^+$ (R = H, **4a**; R = MeO, **4b**; R = F, **4c**; R = $NO_2$, **4d**; see Scheme 3) yielded different results according to the nature of the R group.[14c] The anion appears to be sitting between the two planes (Cp* and arene) with contacts to both ligands. However, whereas for **4d**, the strongest contacts with the arene are with the *para* and *meta* aromatic protons, the situation is different for **4b** and **4c**, for which the strongest contacts with the arene are with the *ortho* protons. An approach of the anion which brings it close to the *meta* and *para* protons of the complexed arene might be expected on the basis of steric grounds. However, it is not evident why $PF_6^-$ would be attracted towards the region of the electronegative O or F atoms, since this approach is sterically less favourable. B3LYP calculations on model systems for the complexes **4** (Cp instead of Cp*) were carried out to shed some light on these results. Instead of focusing on the NPA charges of individual atoms, the contributions from three different parts of the complexes were considered: Ru, Cp, and arene (Table 1). The positive charge of the cation is well distributed with no particular accumulation in a specific region. This explains the overall position of the anion, between the two planes, thus maximizing interactions with all the positively charged centres. Interestingly, the charge of the *ipso* carbon atom is influenced by the nature of R. For R = MeO and F, the *ipso* carbon is strongly positively charged (+0.37 and +0.46,

Table 1. Selected NPA charges of the cation $Ru(Cp)(\eta^6\text{-}C_6H_5R)$.[14c]

| | Ru | Cp | Arene |
|---|---|---|---|
| R = H | 0.21 | 0.32 | 0.47 |
| R = MeO | 0.20 | 0.29 | 0.51 |
| R = F | 0.19 | 0.34 | 0.47 |
| R = $NO_2$ | 0.21 | 0.38 | 0.41 |

  

respectively), while for R = $NO_2$ the accumulation of positive charge is smaller (+0.05). This explains the shift of the anion toward the *ortho* aromatic protons in **4b** and **4c**.

Taken together, all these results show that the charge distribution of the cation and the ability of the anion to approach the positively charged positions are the determining factors in determining the amount of ion-pairing and the geometry of the ion pair. Calculations on model systems of the cation yield a faithful description of the repartition of the electronic density. Charge analysis is usually a sufficiently good indicator of the location of the positively charged area within the complex. This allows a qualitative description of the ion-pairing process. However, this approach suffers from several caveats. First, depending on the model system used in the calculations, the charge analysis may be biased. For example the charge on a phosphorus atom in $PH_3$ is significantly different from that in $PPh_3$ or $PR_3$ (R = alkyl). In the former case, the P atom is anomalously positively charged. Second, calculations on the cation alone do not allow for consideration of the influence of the steric bulk on the ion-pairing process. Certainly the anion seeks the area of positive charge within the complex, but it is not certain that a given position is associated to a short enough contact with the anion for a strong interaction to develop. Only calculations on the actual system with explicit consideration of the counterion would allow such cases to be correctly modelled.

### 1.2. Explicit Calculations of Ion-Pair Geometries

$BF_4^-$ and $BPh_4^-$ are typical counterions used in organometallic chemistry. Even if these anions have a spherical shape, their interaction with a cationic complex is not expected to be similar. The respective size of the two anions is very different with estimated volumes of 49 Å$^3$ for $BF_4^-$ and 284 Å$^3$ for $BPh_4^-$.[10b] In a model describing the ion pair as the result of the interaction between positive and negative charges, the difference in size is likely to introduce variations in the strength of the ion pair. Tighter ion pairs are expected with the smaller anion $BF_4^-$. Moreover, the chemical nature of the boron substituent is also likely to influence the ion-pair structure. Fluorine can be engaged in H-bonding interactions with acidic protons on the ligands, while the phenyl rings in $BPh_4^-$ are prone to develop dispersive interactions with aromatic rings within the ligand set.

These general characteristics are illustrated by a study of the ion pairs of cationic $Ru^{II}$–α-diimine complexes with different counterions.[10b,10c] PGSE and NOE NMR spectroscopic measurements were carried out for complexes [Ru($\eta^6$-cymene){(2-Et-$C_6H_4$)N=C(Me)–C(Me)=N(2-Et-$C_6H_4$)}Cl]X (X = $BF_4^-$, **5a**; X = $BPh_4^-$, **5b**; see Scheme 4). Ion-pairing is the main aggregative process in $CD_2Cl_2$ and solvents with higher relative permittivity. In Table 2 are reported the intensities of the NOE peaks observed in **5a** and **5b** in $CD_2Cl_2$. In **5a**, $^{19}F$,$^1H$ HOESY studies located the anion in ion pairs above the plane containing the C=N imine moieties (Scheme 4). In contrast, the $^1H$-NOESY spectrum for **5b** could not be explained by a single orientation of the $BPh_4^-$ counterion, the anion interacts with the cymene ring and with the diimine ligand to roughly the same extent.

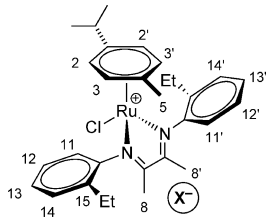


X = $BF_4$, **5a**
X = $BPh_4$, **5b**

Scheme 4. Ion-pairing in $Ru^{II}$ α-diimine complexes.

Table 2. Relative NOE intensities determined by arbitrarily fixing at 1 the NOE(s) between the anion resonance (*o*-H in the case of $BPh_4^-$) and the imine methyl groups.[10b] The numbering scheme is shown in Scheme 4.

| | 8/8′ | $CH_2CH_3$ | $CH_2CH_3$ | 11′ | 2/3 | 7/7′ | 5 |
|---|---|---|---|---|---|---|---|
| **5a** | 1 | 1.23 | 0.46 | 1.78 | 0.17 | 0.10 | 0.25 |
| **5b** | 1 | 0.85 | 0.54 | | 1.47 | 0.38 | 0.70 |

In general, when X-ray structures are available, they constitute good approximate geometries for the optimization of the ion-pair structure. However, in many cases, such information is not available, and different starting geometries have to be considered. It would be very difficult to conduct an extensive conformational search, and approximate geometries for ion pairs are generally drawn on the basis of expected chemical interactions. ONIOM(B3PW91/HF) calculations of the ion-pair structure located for each anion two different geometries of interaction (Figure 1).[10b,10c] The structure with $BF_4^-$ above the Ru(diimine) plane, **5a-I**, is computed to be more stable than the geometry with $BF_4^-$ above the cymene ring, **5a-II**, by 14.9 kcal mol$^{-1}$. There is thus a clear energetic preference for a specific geometry of interaction. Several short contacts between F atoms on $BF_4^-$ and hydrogen atoms on the complex are obtained in **5a-I** (F···H8 2.07 Å, F···H11′ 2.27 Å, F···$CH_2CH_3$ 2.30 Å). These short contacts are in excellent agreement with the relative intensities of the NOE peak (Table 2). It is important to emphasize that the present calculations offer a static picture of the ion pair, whereas the NOE peaks are the result of a dynamic behaviour. In order to take into account the influence of the solvent, the energy of the ONIOM geometries for the ion pairs **5a-I** and **5a-II** were computed at the B3PW91 level within the polarizable continuum method (PCM) approximation ($CH_2Cl_2$ as the solvent). The energy difference is reduced but **5a-I** is still largely more stable than **5a-II** (8.9 kcal mol$^{-1}$). The calculations within the PCM scheme allowed estimating the formation energy of the ion-pair with respect to the separated ions. For **5a-I**, the value of 23.4 kcal mol$^{-1}$ is typical of the energy range of H-bonding interactions.

  

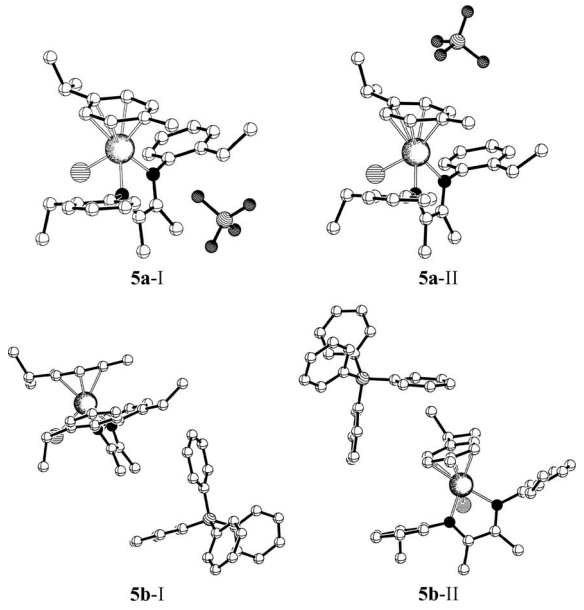


Figure 1. ONIOM(B3PW91/HF) geometries for the ion pair in [Ru($\eta^6$-cymene){(2-Et-$C_6H_4$)N=C(Me)–C(Me)=N(2-Et-$C_6H_4$)}-Cl]X (X = $BF_4^-$, **5a**; X = $BPh_4^-$, **5b**). **I** refers to the structure with the anion above the Ru(diimine) plane, whereas **II** refers to the one with the anion above the cymene ring. H atoms are omitted for clarity.

With $BPh_4^-$ as the counterion, the situation is drastically different. Both structures, **5b-I** and **5b-II** (Figure 1), are computed to have similar stability, **5b-I** being only 1.1 kcal mol$^{-1}$ more stable than **5b-II**. There is thus no preferential geometry of interaction, and the anion occupies the two positions equally. This explains the values of the NOE peak intensities (Table 2). Inclusion of the solvent does not alter the picture, as **5b-I** is computed to be more stable than **5b-II** by 1.7 kcal mol$^{-1}$ within the PCM approximation. The geometries obtained for the ion pairs with $BPh_4^-$ are clearly indicative of dispersive interactions as the driving force for the ion-pairing. This is confirmed by the estimation of the formation energy of the ion pair **5b-I** at 8.7 kcal mol$^{-1}$.

As anticipated, upon consideration of the size of the anion, the ion pair with $BF_4^-$ is thermodynamically more favourable than that with the bigger $BPh_4^-$ anion. However, size arguments are not enough to completely describe the ion-pairing tendency. The nature of the interactions that can be created between the anion and the cation is also an important feature to consider. Inorganic fluorinated anions can interact with acidic sites by formation of H-bonding interactions with stabilization energies sufficient to induce the formation of a specific ion-pair geometry. However, if the difference in acidity between the different protons is not significant, several ion-pair structures of similar energy may coexist. This has been observed in the calculations by Veiros et al. on the ruthenium complexes **4b**–**c** (Scheme 3).[14c] Two different geometries for the ion pair were located, but the energy difference was less than 0.3 kcal mol$^{-1}$ for **4c** and **4d**, whereas the difference was 5.7 kcal mol$^{-1}$ for **4b**. In the latter case, the more stable structure was in agreement with the NMR spectroscopic data, but the difference in behaviour between **4c** and **4d** could not be rationalized by such calculations.

The specific interactions at the origin of the formation of a given ion-pair geometry are also likely to induce dimerization between neutral molecules. Of particular interest are the species involved in the catalytic cycle for transfer hydrogenation with the Ru system developed by Noyori et al. (Scheme 5).[15] A systematic $^1$H PGSE NMR spectroscopic study has been carried out for the Noyori's precatalyst [RuCl($\eta^6$-*p*-cymene){(*S*,*S*)-TsDPEN}] (**6a**) the real catalyst [RuH($\eta^6$-*p*-cymene){(*S*,*S*)-TsDPEN}] (**6b**) and the 16-electron intermediate [Ru($\eta^6$-*p*-cymene){(*S*,*S*)-TsDPEN}] (**6c**).[10d,10e] Compounds **6a**–**c** form dimers at medium-high concentration (10–60 mM). The tendencies to self-aggregate of **6a** and **6b** are identical and higher than that of **6c**. The Gibbs free energy associated with the dimerization process has been calculated from the experimental data to be identical for **6a** and **6b**: $\Delta_r G^0$ = –3.4 kcal mol$^{-1}$ in chloroform and $\Delta_r G^0$ = –2.2 kcal mol$^{-1}$ in 2-propanol.

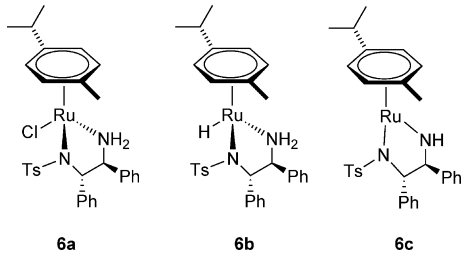


Scheme 5. Structure of the complexes involved in the catalytic cycle for transfer hydrogenation with Noyori's catalyst.

The piano-stool geometry of the complexes allows for an efficient dimerization with an inverted geometry.[16] ONIOM(B3PW91/HF) calculations of the structure of dimers **6a**–**6a**, **6b**–**6b** and **6c**–**6c** (see Figure 2) indicated that the driving force for the aggregation of the neutral molecules is the H-bonding interaction developing between the $SO_2$ group of the tosylate and the $NH_2$ protons (**6a** and **6b**) or the NH group (**6c**). This primary interaction is supplemented by a weaker H-bond between $SO_2$ and one cymene proton. The calculated formation energies for the three dimers (–10.3 kcal mol$^{-1}$ for **6a**–**6a**, –9.2 kcal mol$^{-1}$ for **6b**–**6b**, –8.4 kcal mol$^{-1}$ for **6c**–**6c**) are in qualitative agreement with the experimental data. In particular, the lower dimerization tendency of **6c** is due to the change of geome-

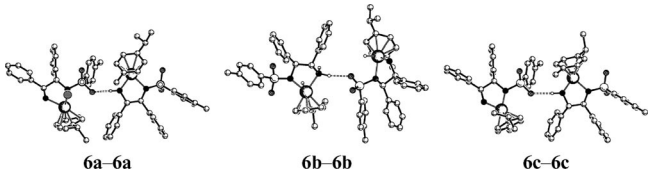


Figure 2. ONIOM(B3PW91/HF) geometries of dimers **6a**–**6a**, **6b**–**6b** and **6c**–**6c**. H atoms not involved in H-bonding are omitted for clarity.

  

try around the 16-electron unsaturated Ru centre, leading to a less efficient interaction of the two piano-stools in an inverted geometry.

## 2. Influence of Ion-Pairing on the Proton Transfer Processes

### 2.1. Influence on Thermodynamics

Heterolytic $H_2$ activation, currently attracting increasing attention, may often go via an acidic $H_2$ complex.[17] Coordination of $H_2$ is usually favoured for electrophilic cationic complexes, where the interaction between the metal and $H_2$ is dominated by the σ-donation from $H_2$ thus increasing its acidity. The aqua complex $[IrH(bq\text{-}H)(OH_2)(PPh_3)_2]BF_4$ (bq-H = 7,8 benzoquinolate) (**7a**) reacts with $H_2$ to give a cationic $H_2$ complex, **8**, which is characterized in detail[18] and whose reaction with a base leads to deprotonation of the $H_2$ ligand to form a neutral dihydride **9** (Scheme 6). The ligand 2-aminobenzoquinolate (bq-$NH_2$) was designed to favour heterolysis of $H_2$. The amino group, located on the bq framework near the $H_2$ binding site, can act as an intramolecular base causing proton abstraction from $H_2$. The rigidity of the bq framework prevents $NH_2$ from directly binding to the metal, which would block the $H_2$ binding site. Indeed, the aqua complex $[IrH(bq\text{-}NH_2)(OH_2)(PPh_3)_2]BF_4$ (**7b**) reacts with $H_2$ to give, not the corresponding $H_2$ complex, **10**, but, by heterolytic activation, the cationic dihydride, **11** (Scheme 6).[19]

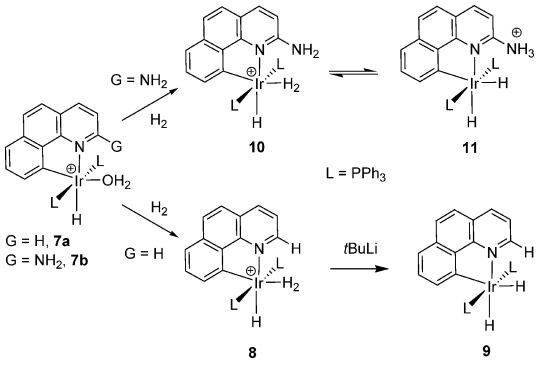


Scheme 6. Influence of the nature of the 2-group G on the benzoquinolate ligand in the deprotonation of coordinated $H_2$ to $Ir(bq\text{-}G)(H)(PPh_3)_2^+$.

In order to gain insight into the geometrical parameters associated with the dihydrogen bond between the hydride and the $NH_3^+$ group,[20]B3PW91 geometry optimizations of model systems of **10** and **11** were carried out (L = $PH_3$).[19] The dihydrogen bond N–H···H–Ir in **11** was computed to be very short (1.379 Å), and the $H_2$ complex **10** is more stable than the experimentally observed product **11** by 14.4 kcal mol$^{-1}$. The phosphane $PH_3$ used in the calculations is too electron-releasing and the hydride in **11** is artificially too basic, which leads to complete proton transfer from the $NH_3^+$ group. As a matter of fact, when the experimental phosphane is changed from $PPh_3$ to more basic ones such as $PBu_3$, $PMePh_2$ or $PMe_2Ph$, the equilibrium between complexes **10** and **11** is shifted toward the $H_2$ complex **10**.[19] Moreover, when the electron-releasing character of the phosphane is reduced in the calculations by using $PF_3$ instead of $PH_3$, the dihydrogen-bonded isomer **11** is now more stable than the $H_2$ complex **10** by 1.0 kcal mol$^{-1}$, and the dihydrogen bond has a more typical value (1.613 Å).

There seems to be a direct effect of the electronic influence of the phosphane on the position of the equilibrium between **10** and **11**; basic phosphanes favour the $H_2$ complex. However, the Tolman electronic parameter (TEP)[21] for $PH_3$ (2083.2 cm$^{-1}$) is greater than that for $PPh_3$ (2068.9 cm$^{-1}$), thus indicating that the latter phosphane is more basic. Consequently the $H_2$ complex **10** should also be observed with $PPh_3$ as a phosphane. The topology of the electrostatic potential in the bq-$NH_2$ plane for the two isomers **10** and **11** with $PH_3$ indicated a potential influence of the steric bulk of the phosphane in the interaction with the counterion $BF_4^-$.[11a] To achieve similar cation–anion interaction, $BF_4^-$ is to be situated closer to the metal centre and toward the $H_2$ ligand in **10**, whereas in **11**, the interaction is more efficient with the $NH_3^+$ group and the vicinal aromatic proton.

This is confirmed by ONIOM(B3PW91/UFF) calculations of the ion-pair structures **10**-$BF_4$ and **11**-$BF_4$ (Figure 3), where the experimental phosphane $PPh_3$ has been considered.[11a] In **10**-$BF_4$, there are two short H···F contacts between the cation and anion, one with the $H_2$ ligand (H···F 2.068 Å) and the other with the $NH_2$ group (H···F 1.781 Å). In **11**-$BF_4$, there are three short H···F contacts: two are with $NH_3^+$ (H···F 1.652 and 1.661 Å) and one is with H3 on the benzoquinolate ligand (H···F 2.219 Å). Complex **11**-$BF_4$ is now computed to be marginally less stable than **10**-$BF_4$ by 0.4 kcal mol$^{-1}$, as a result of an optimal arrangement for anion–cation-specific interactions in **11**-$BF_4$. Ion-pairing is thus responsible for the unexpected experimental observation of **11** in the case of L = $PPh_3$. With close contacts between acidic protons and $BF_4^-$, strong electronic preference for the dihydrogen complex may be significantly reduced. Electronic and steric components of the ion-pairing energy contribute to the effect with a more efficient interaction and a weaker steric repulsion in the hydride isomer **11**. As a final experimental test of the

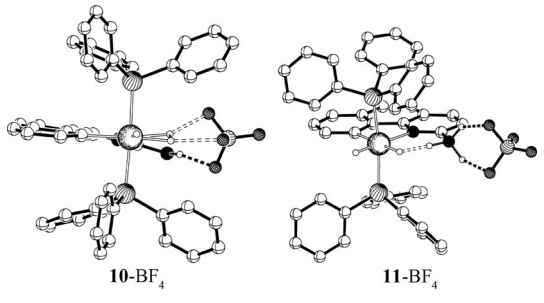


Figure 3. ONIOM(B3PW91/UFF) structures of the ion pair between $BF_4^-$ and the dihydrogen complex **10** and the product of heterolytic $H_2$ cleavage, **11**. H atoms not involved in H-bonding are omitted for clarity.

  

ion-pairing effect on the position of the equilibrium between **10** and **11**, the complex with the very bulky and very basic phosphane $PCy_3$ was synthesized and the dihydrogen bonded isomer **11** was obtained.[11a]

### 2.2. Influence on Kinetics

There is an increasing number of experimental studies where a direct effect of the "inert" counterion is observed on the kinetics of the reaction under study. The kinetics of reaction of the dihydrogen complex *trans*-$[FeH(\eta^2\text{-}H_2)(dppe)_2]^+$ with an excess of $NEt_3$ to form *cis*-$[FeH_2(dppe)_2]$ is accelerated by $BF_4^-$ and $PF_6^-$ and decelerated in the presence of $BPh_4^-$.[22] B3LYP calculations by Lledós and Maseras[22] of the reaction mechanism without explicit inclusion of the counterion highlighted the different steps along the proton transfer process. The latter is effective through an intermediate with a stretched $H_2$ ligand (1.211 Å) coordinated in an end-on way between the Fe centre and the nitrogen atom of $NMe_3$ (3.0 kcal mol$^{-1}$ with respect to the reactant in THF). The energy-demanding steps are the separation of *trans*-$[FeH_2(dppe)_2]$ and $HNMe_3^+$ (11.5 kcal mol$^{-1}$ in THF) and the *trans–cis* isomerization (17.9 kcal mol$^{-1}$ in THF).

Calculations (B3LYP/PCM) with $BF_4^-$ as a counterion indicated formation of a stable ion pair in which the anion interacts with the $H_2$ ligand. However, the geometry of the ion pair allows for $NMe_3$ to interact with the $H_2$ ligand to yield an intermediate similar to the one located in the mechanism without counterion. The energy benefit of the ion-pairing interaction is preserved, as this intermediate is 15.0 kcal mol$^{-1}$ more stable than the separated reactants in THF. Moreover, the proton transfer from $H_2$ to $NMe_3$ is accompanied by the formation of the ion pair $[HNMe_3][BF_4]$, thus cancelling out the energy cost of product separation after the transfer process. The activation barrier is now reduced to the isomerization of the neutral dihydride, which explains the acceleration observed with $BF_4^-$. The results are similar with $PF_6^-$ as a counterion. For these inorganic fluorinated anions, the proton transfer is eased by creation of F···H interactions along the pathway, stabilizing both the reactants and the products. In contrast, for $BPh_4^-$ as a counterion, there is formation of a stable ion pair but with a geometry precluding any proton transfer from $H_2$ to the base. Two phenyl rings of the anion, involved in C–H···π interactions with the hydrogen atoms on the chelating phosphane ligands, shield the $H_2$ ligand, and the base is not able to interact; this explains the decelerating effect. The ion pair has to be broken, and there is no creation of an ion pair with the protonated base to stabilize the separation of the products.

Nevertheless, depending on the network of interactions at the origin of the formation of the ion pair, an inorganic fluorinated anion may have a decelerating effect on a proton transfer process. The $^{19}F,^1H$ HOESY spectra of the hydride cluster $[W_3S_4H_3(dmpe)_3]^+$ in $CD_2Cl_2$ solution indicate the formation of ion pairs with $BF_4^-$ with a well-defined interionic structure with close contact between the hydride and the fluorine atoms.[23] In an excess of $BF_4^-$, the rate of proton transfer to the hydride from HCl is decreased. B3LYP calculations on $[W_3S_4H_3(PH_3)_6]^+$ as a model for the cluster were carried out to shed light on the anion effect.[23] In the absence of the anion, the calculations revealed the formation of a W–H···H–Cl adduct with a very short dihydrogen bond (H···H 1.36 Å). When the anion $BF_4^-$ is introduced in the calculations, an ion pair is obtained with three short W–H···F–B contacts (2.67, 2.98 and 3.19 Å), in agreement with the NMR spectroscopic observations. As a result, the interaction between W–H and H–Cl is less efficient, because the hydride is shielded by the anion. Consequently, the W–H···H–Cl contact is elongated to a value (2.68 Å) precluding any proton transfer. Moreover, the calculations revealed that the formation of the adduct $ClH\cdots BF_4^-$ is thermodynamically favoured, thus leading to a decrease in the effective HCl concentration. $BF_4^-$ acts also as a scavenger for the HCl molecules, and this process contributes to the deceleration.

The preceding examples have highlighted the influence of the counterion on the kinetics through stabilization or destabilization of some intermediates. However, there is potentially another way to influence the rate of a reaction, i.e. by acting on the energy of the transition state. Formation of a specific ion-pair structure in the transition state may open up new reaction pathways, and thus may lead to a significant anion effect on reactivity. An illustrative example is provided by the theoretical study by Lledós and Ujaque of the reaction mechanism of the gold(I)-phosphane-catalyzed hydroamination of 1,3-dienes (Scheme 7).[24]

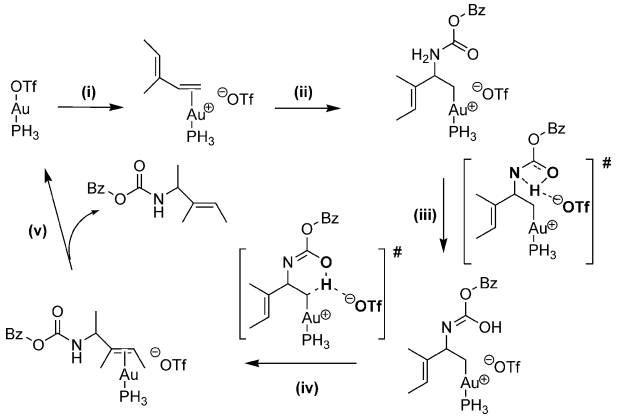


Scheme 7. Computed reaction pathway for the hydroamination reaction of 1,2-dimethylbutadiene with benzyl carbamate. The various steps are: (i) coordination of the diene, (ii) external nucleophilic attack by the carbamate, (iii) triflate-assisted tautomerization, (iv) triflate-assisted proton transfer to the unsaturated carbon atom, (v) product release.[24]

The most striking result of this computational study is the crucial role played by the triflate anion. The direct proton transfer from nitrogen to carbon without anion assistance is computed with an activation barrier of 51.5 kcal mol$^{-1}$. The activation barrier for the very same process is reduced to 38.7 kcal mol$^{-1}$ with assistance by the

  

triflate anion. However, an even lower activation barrier is obtained (26.2 kcal mol$^{-1}$) in a proton transfer from N to C occurring in two consecutive anion-assisted proton transfers: from N to O and from O to C (Scheme 7). In these two steps, the influence of the anion is fully developed in the transition state, but not in the intermediates.

In the gold-catalyzed cycloisomerization of bromoallenyl ketones, the nature of the counterion of the gold(I) metal centre influences the regiochemistry of the cyclic product (Scheme 8).[25] DFT calculations of the reaction mechanism with Au(PH$_3$)X as a model for the catalyst illustrated the influence of the anion. The crucial step to determine the regiochemistry is a 1,2-H or 1,2-Br shift in the cyclic product bonded to Au. The 1,2-Br shift is not influenced by the nature of X, whereas the 1,2-H shift is anion-dependent. With X = triflate, the activation barrier for the 1,2-H shift is computed to be lower than the barrier for 1,2-Br shift. The situation is the opposite for $BF_4^-$ and $SbF_6^-$, in excellent agreement with the experimental results (Scheme 8). The key influence of the anion is thus rationalized by the calculations as the capacity to stabilize the transition state for 1,2-H shift through creation of an efficient network of H-bonds between the anion and the migrating proton.

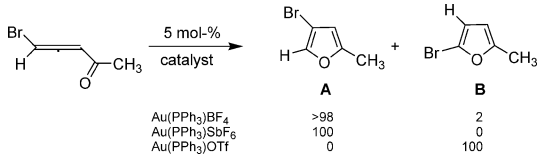


Scheme 8. Influence of the counterion on the regiochemistry of cycloisomerization of bromoallenyl ketone.[25]

The possibility to favour a proton transfer by stabilizing the transition state upon creation of an efficient H-bonding network with the counterion is nicely illustrated by the anion effect on some imidazolium salt metallation reactions.[26] The use of an N-heterocyclic carbene as supporting ligand in homogeneous catalysis has considerably increased during the last ten years.[27] When functionalized architectures are considered, mild conditions for carbene transfer to the metal centre are preferred over the traditional deprotonation by a strong base. C–H activation of functionalized imidazolium **12** at electron-rich transition-metal centres is a possibility (Scheme 9). However, the reaction does not always yield metallation at the expected C2-position of the imidazolium ring (**13**, Scheme 9). The product of metallation at the C5-position, the abnormal carbene **14**, is obtained in some cases. Even more intriguing is the fact that the ratio between **13** and **14** depends on the nature of the counterion and on the nature of the substituent R on nitrogen (Table 3).[11b,11c]

Formation of the carbene at the C2-position is intrinsically preferred thermodynamically, and B3PW91 calculations on the free ligand yielded an energy difference of 15 kcal mol$^{-1}$ in favour of the formation of the C2-carbene.[11b] This energy difference is reduced to 10.1 kcal mol$^{-1}$ with ONIOM(B3PW91/UFF) calculations of the cations **13** and **14**, the C2-product still being more

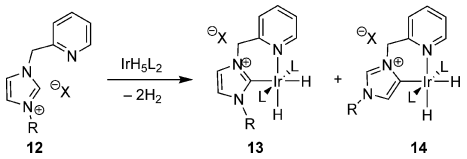


Scheme 9. Formation of normal and abnormal carbenes from reaction of imidazolium with iridium polyhydride (L = PPh$_3$).

Table 3. Ratio between the normal, **13**, and the abnormal, **14**, carbene complexes as a function of the N-substituent and the nature of the counterion (Scheme 9).

| R | X | **13** | **14** |
|---|---|---|---|
| Me | Br | 91 | 9 |
| Me | OAc | 80 | 20 |
| Me | $BF_4$ | 45 | 55 |
| Me | $PF_6$ | 50 | 50 |
| Me | $SbF_6$ | 11 | 89 |
| *i*Pr | Br | 84 | 16 |
| *i*Pr | $BF_4$ | 0 | 100 |

stable. There is no particular stabilizing effect associated to creating an Ir–C bond at the C5-position.

Calculations of ion-pair structures for **13** and **14** with $Br^-$ and $BF_4^-$ resulted in almost the cancellation of the energy difference. The C2-product is only 1.6 kcal mol$^{-1}$ (with respect to 3.8 kcal mol$^{-1}$) more stable than the C5-product with $BF_4^-$ (with respect to $Br^-$). This drastic change in thermodynamic stability originates from the different H-bond networks present in each ion-pair structure (Figure 4). In the C5-product, the very acidic C2–H bond is still available to create efficient H-bonding interactions with the counterion. These stabilizing interactions compensate for the less efficient bonding of C5 to the metal centre.

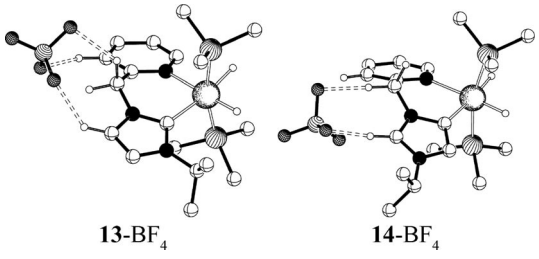


Figure 4. ONIOM(B3PW91/UFF) ion-pair structures for the normal and abnormal carbenes with the $BF_4^-$ counterion. H atoms not involved in H-bonding are omitted for clarity, only the *ipso* carbon on PPh$_3$ is shown.

Formation of the ion pair allows for thermodynamic access to the abnormal carbene. However, the anion effects shown in Table 3 can not be rationalized only by invoking formation of an ion pair in the product. In particular, the critical influence of the bulk of both the anion and the R group on the nitrogen can not be accounted for. The computational study of the reaction pathways leading to the normal and abnormal carbenes was carried out on a model system consisting of IrH$_3$(PMe$_3$)$_2$ and the *N*,*N*′-dimethylimidazolium cation in the presence of $X^-$ where X = $BF_4$ or Br.[11c] In the transition state for metallation at the C2-

  

position, the anion explicitly interacts with the migrating hydrogen and follows the hydrogen in its transfer to the hydride (Figure 5). The product of the C–H bond breaking is an $Ir^{III}$–dihydrogen complex, and the reaction is best described as a proton transfer. The capacity of the anion to create an efficient H-bonding interaction with a particular hydrogen atom and the size of the anion are critical parameters in the anion-assisted proton migration. In the transition state for metallation at the C5-position, the anion is not directly involved in the reaction (Figure 5), and the mechanism is a classical C–H activation with formation of an $Ir^{V}$ tetrahydride intermediate. The activation barrier for reaction at C2 is thus computed to be lower than that for activation at C5 for $Br^-$ and the opposite trend is obtained with $BF_4^-$, in excellent agreement with the experimental observations.

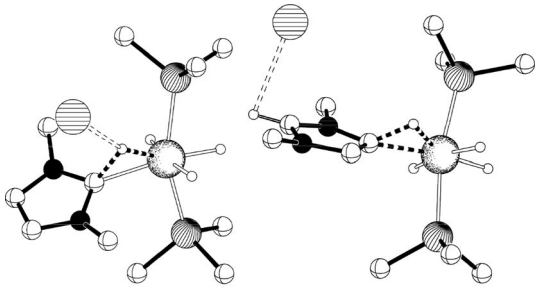


Figure 5. Structure of the transition state for metallation at the C2-position (left) and at the C5-position (right) in the presence of $Br^-$ as the counterion. H atoms not involved in H-bonding are omitted for clarity.

## Conclusions

The calculations performed to study ion-pairing phenomena in organometallic chemistry have highlighted the principal aspects to consider. The charge distribution of the cation itself is already a good indicator of potential sites for anion–cation interactions. Such information is relatively easy to obtain and, generally, the accumulation of positive charge within a complex is not at the metal centre but more often on a particular ligand. However, in addition to the electrostatic attraction, ion-pairing is also the result of the creation of specific interactions between the anion and the cation. In this respect, inorganic fluorinated anions, traditionally used because they are considered to be noncoordinating, participate in H-bonding networks favouring a specific geometry for the ion pair. A very nice recent example is given by the combined experimental and theoretical study of ion-pairing in cationic olefin–gold(I) complexes by Macchioni and co-workers.[28] For tetraarylborate anions, dispersive interactions are the main contributors to the ion-pairing process, and several isoenergetic ion pairs are observed. The computational description of such ion pairs requires the use of a hybrid method such as ONIOM to take into account the steric properties of the system. Depending on the nature of the interactions, hybrid QM/MM or QM/QM′ approaches can be used. ONIOM(DFT/HF) calculations are particularly adapted to describe the H-bonding interactions with fluorine atoms, while ONIOM(DFT/MM) calculations give a good description of the ion-pairing with $BPh_4^-$. The choice of the partition between the two descriptions is also an important aspect of such calculations.

The influence of the anion on the reactivity is particularly important in proton transfer processes. In these situations, the anion, in particular $BF_4^-$, often interacts with the reactive site. This proximity affords stabilization of intermediates and/or transition states. The driving force is the creation of H-bonding interactions with the migrating protons. Experimentally, apart from effects on the distribution of rates and/or products, very little information is available on the influence of the anion. Computational studies of the reaction mechanism with and without the anion included offer a wealth of information. It is often the case that the anion opens new reaction pathways, and certainly more and more surprising results are to be described in the future.

## Acknowledgments

This work is the result of a very fruitful collaboration with Alceo Macchioni, and none of it would have been done without his expertise in the NMR spectroscopic study of ion-pairing. I would also like to thank Robert H. Crabtree and Odile Eisenstein for their constant support over the last ten years and for the numerous stimulating discussions.

[1] a) A. Macchioni, *Eur. J. Inorg. Chem.* **2003**, 195–205; b) A. Macchioni, *Chem. Rev.* **2005**, *105*, 2039–2073; c) G. Bellachioma, G. Ciancaleoni, C. Zuccaccia, D. Zuccaccia, A. Macchioni, *Coord. Chem. Rev.* **2008**, *252*, 2224–2238; d) A. Macchioni, G. Ciancaleoni, C. Zuccaccia, D. Zuccaccia, *Chem. Soc. Rev.* **2008**, *37*, 479–489.

[2] a) P. S. Pregosin, P. G. A. Kumar, I. Fernández, *Chem. Rev.* **2005**, *105*, 2977–2998; b) P. S. Pregosin, *Prog. Nuc. Magn. Reson. Spectrosc.* **2006**, *49*, 261–288.

[3] E. Y.-X. Chen, T. J. Marks, *Chem. Rev.* **2000**, *100*, 1391–1434.

[4] a) R. Fusco, L. Longo, F. Masi, F. Garbassi, *Macromol. Rapid Commun.* **1997**, *18*, 433–441; b) R. Fusco, L. Longo, F. Masi, F. Garbassi, *Macromolecules* **1997**, *30*, 7673–7685; c) R. Fusco, L. Longo, A. Proto, F. Masi, F. Garbassi, *Macromol. Rapid Commun.* **1998**, *19*, 257–262.

[5] a) G. Lanza, I. L. Fragalà, T. J. Marks, *J. Am. Chem. Soc.* **1998**, *120*, 8257–8258; b) G. Lanza, I. L. Fragalà, *Top. Catal.* **1999**, *7*, 45–60; c) G. Lanza, I. L. Fragalà, T. J. Marks, *J. Am. Chem. Soc.* **2000**, *122*, 12764–12777.

[6] a) M. S. W. Chan, K. Vanka, C. C. Pye, T. Ziegler, *Organometallics* **1999**, *18*, 4624–4636; b) K. Vanka, M. S. W. Chan, C. C. Pye, T. Ziegler, *Organometallics* **2000**, *19*, 1841–1849; c) M. S. W. Chan, T. Ziegler, *Organometallics* **2000**, *19*, 5182–5189; d) Z. Xu, K. Vanka, T. Firman, A. Michalak, E. Zurek, C. Zhu, T. Ziegler, *Organometallics* **2002**, *21*, 2444–2453; e) Z. Xu, K. Vanka, T. Ziegler, *Organometallics* **2004**, *23*, 104–116; f) T. Wondimagegn, K. Vanka, Z. Xu, T. Ziegler, *Organometallics* **2004**, *23*, 2651–2657.

[7] a) I. E. Nifant'ev, L. Y. Ustynyuk, D. N. Laikov, *Organometallics* **2001**, *20*, 5375–5393; b) I. E. Nifant′ev, L. Y. Ustynyuk, D. V. Besedin, *Organometallics* **2003**, *22*, 2619–2629; c) L. Y. Ustynyuk, E. A. Fushman, A. Razavi, *Kinet. Catal.* **2006**, *47*, 213–220.

[8] a) A. Correa, L. Cavallo, *J. Am. Chem. Soc.* **2006**, *128*, 10952–10959; b) C. Alonso-Moreno, S. J. Lancaster, J. A. Wright,

  

D. L. Hughes, C. Zuccaccia, A. Correa, A. Macchioni, L. Cavallo, M. Bochmann, *Organometallics* **2008**, *27*, 5474–5487.

[9] X. Yang, C. L. Stern, T. J. Marks, *J. Am. Chem. Soc.* **1994**, *116*, 10015–10031.

[10] a) A. Macchioni, C. Zuccaccia, E. Clot, K. Gruet, R. H. Crabtree, *Organometallics* **2001**, *20*, 2367–2373; b) D. Zuccaccia, S. Sabatini, G. Bellachioma, G. Cardaci, E. Clot, A. Macchioni, *Inorg. Chem.* **2003**, *42*, 5465–5467; c) D. Zuccaccia, G. Bellachioma, G. Cardaci, G. Ciancaleoni, C. Zuccaccia, E. Clot, A. Macchioni, *Organometallics* **2007**, *26*, 3930–3946; d) D. Zuccaccia, E. Clot, A. Macchioni, *New J. Chem.* **2005**, *29*, 430–433; e) G. Ciancaleoni, C. Zuccaccia, D. Zuccaccia, E. Clot, A. Macchioni, *Organometallics* **2009**, *28*, 960–967.

[11] a) K. Gruet, E. Clot, O. Eisenstein, D. H. Lee, B. Patel, A. Macchioni, R. H. Crabtree, *New J. Chem.* **2003**, *27*, 80–87; b) A. Kovacevic, S. Gründemann, J. R. Miecznikowski, E. Clot, O. Eisenstein, R. H. Crabtree, *Chem. Commun.* **2002**, 2580–2581; c) L. N. Appelhans, D. Zuccaccia, A. Kovacevic, A. R. Chianese, J. R. Miecznikowski, A. Macchioni, E. Clot, O. Eisenstein, R. H. Crabtree, *J. Am. Chem. Soc.* **2005**, *127*, 16299–16311.

[12] a) B. D. Alexander, B. J. Johnson, S. M. Johnson, P. D. Boyle, N. C. Kann, L. H. Pignolet, *Inorg. Chem.* **1987**, *26*, 3506–3513; b) I. A. Guzei, A. L. Rheingold, D. H. Lee, R. H. Crabtree, *Z. Kristallogr. - New Cryst. Struct.* **1998**, *213*, 585.

[13] E. Clot, O. Eisenstein, T. Dubé, J. W. Faller, R. H. Crabtree, *Organometallics* **2002**, *21*, 575–580.

[14] a) D. Schott, P. S. Pregosin, L. F. Veiros, M. J. Calhorda, *Organometallics* **2005**, *24*, 5710–5717; b) D. Nama, D. Schott, P. S. Pregosin, L. F. Veiros, M. J. Calhorda, *Organometallics* **2006**, *25*, 4596–4604; c) A. Moreno, P. S. Pregosin, L. F. Veiros, A. Albinati, S. Rizzato, *Chem. Eur. J.* **2008**, *14*, 5617–5629.

[15] a) S. Hashiguchi, A. Fujii, J. Takehara, T. Ikariya, R. Noyori, *J. Am. Chem. Soc.* **1995**, *117*, 7562–7563; b) K. J. Haack, S. Hashiguchi, A. Fukii, T. Ikariya, R. Noyori, *Angew. Chem. Int. Ed. Engl.* **1997**, *36*, 285–288.

[16] a) H. Brunner, *Angew. Chem. Int. Ed.* **1999**, *38*, 1194–1208; b) H. Brunner, *Eur. J. Inorg. Chem.* **2001**, 905–912.

[17] D. M. Heinekey, W. J. Oldham Jr, *Chem. Rev.* **1993**, *93*, 913–926.

[18] R. H. Crabtree, M. Lavin, L. Bonneviot, *J. Am. Chem. Soc.* **1986**, *108*, 4032–4037.

[19] D.-H. Lee, B. P. Patel, E. Clot, O. Eisenstein, R. H. Crabtree, *Chem. Commun.* **1999**, 297–298.

[20] R. H. Crabtree, P. E. M. Siegbahn, O. Eisenstein, A. L. Rheingold, T. F. Koetzle, *Acc. Chem. Res.* **1996**, *29*, 348–354.

[21] A. Tolman, *Chem. Rev.* **1977**, *77*, 313–348.

[22] a) M. G. Bassallote, M. Besora, J. Durán, M. J. Fernández-Trujillo, A. Lledós, M. A. Máñez, F. Maseras, *J. Am. Chem. Soc.* **2004**, *126*, 2320–2321; b) M. G. Bassallote, M. Besora, C. E. Castillo, M. J. Fernández-Trujillo, A. Lledós, F. Maseras, M. A. Máñez, *J. Am. Chem. Soc.* **2007**, *129*, 6608–6618; c) see also M. Besora, A. Lledós, F. Maseras, *Chem. Soc. Rev.* **2009**, *38*, 957–966 for theoretical work on protonation of transition-metal hydrides.

[23] A. G. Algarra, M. G. Bassallote, M. J. Fernández-Trujillo, R. Llusar, V. S. Safont, C. Vicent, *Inorg. Chem.* **2006**, *45*, 5774–5784.

[24] G. Kovács, G. Ujaque, A. Lledós, *J. Am. Chem. Soc.* **2008**, *130*, 853–864.

[25] Y. Xia, A. S. Dubnik, V. Gevorgyan, Y. Li, *J. Am. Chem. Soc.* **2008**, *130*, 6940–6941.

[26] a) S. Gründemann, A. Kovacevic, M. Albrecht, J. W. Faller, R. H. Crabtree, *Chem. Commun.* **2001**, 2274–2275; b) S. Gründemann, A. Kovacevic, M. Albrecht, J. W. Faller, R. H. Crabtree, *J. Am. Chem. Soc.* **2002**, *124*, 10473–10481.

[27] a) W. A. Herrmann, *Angew. Chem. Int. Ed.* **2002**, *41*, 1290–1309; R. Corberán, E. Mas-Marzá, E. Peris, *Eur. J. Inorg. Chem.* **2009**, 1700–1716.

[28] D. Zuccaccia, L. Belpassi, F. Tarantelli, A. Macchioni, *J. Am. Chem. Soc.* **2009**, *131*, 3170–3171.

Received: February 14, 2009
Published Online: April 29, 2009

  